JACS
JOURNAL OF THE AMERICAN CHEMICAL SOCIETY
Article
pubs.acs.org/JACS

Synthesis of Functionalized 1,4-Azaborinines by the Cyclization of Di-*tert*-butyliminoborane and Alkynes

Marius Schäfer,[†] Nicholas A. Beattie,[‡] K. Geetharani,[†,⊥] Julian Schäfer,[§] William C. Ewing,[†] Mirjam Krahfuß,[†] Christian Hörl,[†] Rian D. Dewhurst,[†] Stuart A. Macgregor,*[,‡] Christoph Lambert,*[,§] and Holger Braunschweig*[,†]

[†]Institut für Anorganische Chemie, Julius-Maximilians-Universität Würzburg, Am Hubland, 97074 Würzburg, Germany
[‡]Institute of Chemical Sciences, Heriot-Watt University, Edinburgh EH14 4AS, U.K.
[§]Insitute für Organische Chemie, Julius-Maximilians-Universität Würzburg, Am Hubland, 97074 Würzburg, Germany

Supporting Information

ABSTRACT: Di-*tert*-butyliminoborane is found to be a very useful synthon for the synthesis of a variety of functionalized 1,4-azaborinines by the Rh-mediated cyclization of iminoboranes with alkynes. The reactions proceed via [2 + 2] cycloaddition of iminoboranes and alkynes in the presence of $[RhCl(PiPr_3)_2]_2$, which gives a rhodium η^4-1,2-azaborete complex that yields 1,4-azaborinines upon reaction with acetylene. This reaction is compatible with substrates containing more than one alkynyl unit, cleanly affording compounds containing multiple 1,4-azaborinines. The substitution of terminal alkynes for acetylene also led to 1,4-azaborinines, enabling ring substitution at a predetermined location. We report the first general synthesis of this new methodology, which provides highly regioselective access to valuable 1,4-azaborinines in moderate yields. A mechanistic rationale for this reaction is supported by DFT calculations, which show the observed regioselectivity to arise from steric effects in the B−C bond coupling en route to the rhodium η^4-1,2-azaborete complex and the selective oxidative cleavage of the B−N bond of the 1,2-azaborete ligand in its subsequent reaction with acetylene.

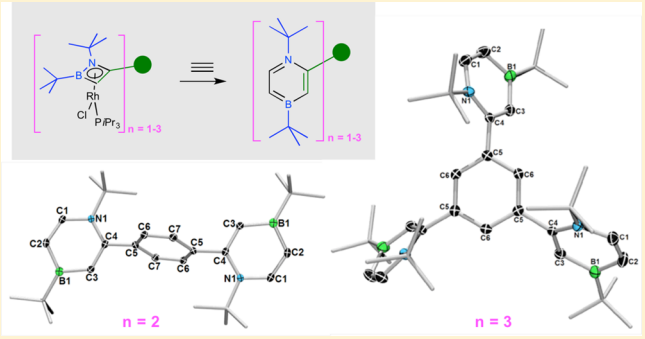

INTRODUCTION

BN/CC isosterism has attracted a great deal of attention in recent years because of the isoelectronic nature of BN and CC units in conventional organic compounds.[1] Benzene-like cyclics wherein two of the carbon atoms have been replaced by one boron and one nitrogen atom are known as azaborinines and have three isomeric forms: 1,2-, 1,3-, and 1,4-azaborinines. Of the three, 1,2-azaborinines have been known the longest, having been reported in the early 1960s by Dewar[2] and White.[3] Recent years have witnessed spectacular development in the chemistry of these compounds by the groups of Ashe,[4] Piers,[5] Yamaguchi,[6] Perepichka[7] and Liu,[8] extending the initial synthetic breakthroughs (the unsubstituted parent 1,2-dihydro-1,2-azaborinine was isolated only recently[9]) into more applied areas such as biomedical research and materials science. Comparatively little research has focused on the chemistry of 1,3- and 1,4-azaborinines[10,11] because of a lack of suitable methodologies for their syntheses.

The development of 1,4-azaborinines has been predominantly limited to polycyclic frameworks (Figure 1, top), such as the anthracene analogue first reported by Maitlis.[12] A few years later, the same anthracene core was synthesized by Clark via the reaction of *o*,*o*′-dilithiodiphenylmethylamine with $BF_3{\cdot}Et_2O$ followed by treatment with mesityllithium.[13] Kawashima and co-workers extended these systems, reporting the syntheses, optical properties, and reactivities of polycyclic 1,4-azaborinines and related polycycles.[14] Though several approaches exist for

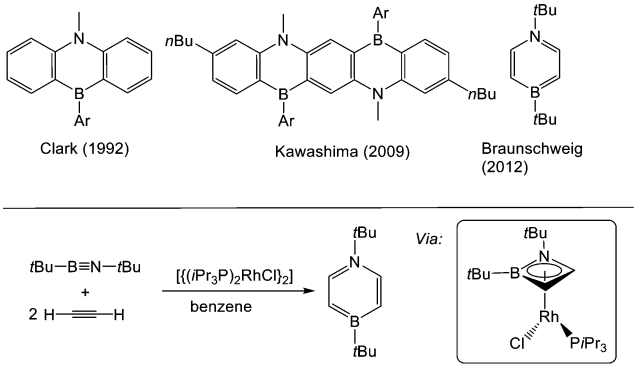

Figure 1. (top) Isolated 1,4-azaborinines. (bottom) Rh-mediated synthesis of a 1,4-azaborinine via a 1,2-azaborete complex.

Received: April 22, 2016
Published: June 10, 2016

DOI: 10.1021/jacs.6b04128
J. Am. Chem. Soc. 2016, 138, 8212−8220

the syntheses of such polycyclic systems,[15] strategies for the syntheses of monocyclic derivatives have only recently been revealed. In 2012, we reported a new synthetic route to monocyclic 1,4-azaborinines through Rh-catalyzed cyclization reactions of alkynes and iminoboranes.[11] These reactions involve tandem [2 + 2]/[2 + 4] cycloaddition of the iminoborane *t*BuB≡N*t*Bu (**1**) with acetylene in a sequence involving rupture of the B≡N bond. We recently extended this approach, showing the system to be capable of selectively producing 1,2-azaborinines through simple variation of the alkyne.[16]

The isolation of a rhodium 1,2-azaborete complex from reactions leading to the formation of 1,4-azaborinines led us to envisage the use of this intermediate in the syntheses of a much wider range of functionalized materials with fine regiochemical control. In this paper we describe these efforts and likewise demonstrate the formation of unusual bis- and tris-1,4-azaborinines through judicious choice of the alkyne. In total, this work vastly extends the range of known compounds within this class of fascinating BN/CC isosteric aromatic structures.

RESULTS AND DISCUSSION

Synthesis of Phenyl and Ferrocenyl 1,4-Azaborinine Derivatives. The recent work on the catalytic pathways leading to functionalized 1,2-azaborinines led us to investigate the regioselectivity of this reaction in more detail, particularly using terminal alkynes. The phenyl-substituted 1,4-azaborinine **4** can be synthesized in moderate yield in two steps. The first is a stoichiometric reaction of iminoborane **1** and phenylacetylene in the presence of $[RhCl(PiPr_3)_2]_2$ (**2**), yielding the rhodium η^4-1,2-azaborete intermediate **3**. When this complex is then reacted with acetylene, 2-phenyl-1,4-azaborinine **4** is formed in moderate yield (Scheme 1). Compounds **3** and **4** were characterized by standard spectroscopic methods, and their solid-state structures were confirmed by single-crystal X-ray diffraction.

Scheme 1. Synthesis of Rhodium η^4-1,2-Azaborete Complexes 3 and 5 and Substituted 1,4-Azaborinines 4 and 6; the Numbering Scheme for Ring Substituents Is Also Provided

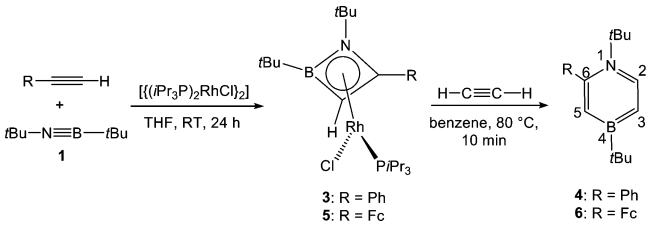

During the course of the reaction, the ^{11}B NMR shift changed from 5 ppm in **1** to 25 ppm in **3** and finally to 46 ppm in **4**, in agreement with previously reported data for 1,4-azaboretes and 1,4-azaborinines.[11] The ^1H NMR spectra of **3** and **4** display resonances characteristic of their phenyl groups (**3**: δ = 7.86 and 7.01 ppm; **4**: δ = 7.17 and 7.01 ppm) as well as BN heterocycle ring protons (**3**: 3.24 ppm; **4**: 7.84, 6.74, and 6.62 ppm).

Orange crystals of **3** and colorless crystals of **4** suitable for single-crystal X-ray crystallography (Figure 2) were obtained by recrystallization from saturated benzene solutions. The N–C, B–C, and C–C bond lengths in **4** are comparable to those of

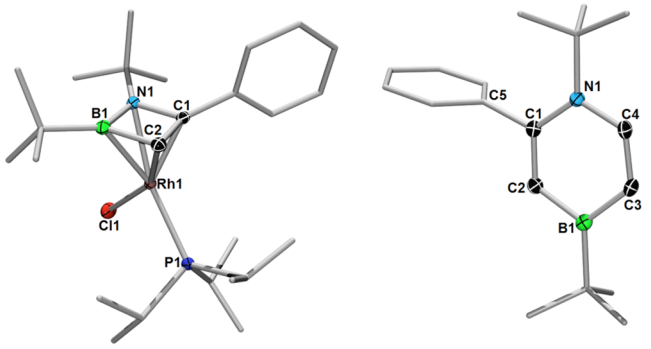

Figure 2. Molecular structures of $[\eta^4$-1,2-{B(*t*Bu)N(*t*Bu)C(Ph)C(H)}RhCl($PiPr_3$)] (**3**) and 1,4-di-*tert*-butyl-2-phenyl-1,4-azaborinine (**4**). The two crystallographically independent molecules in the asymmetric unit of **4** have nearly identical geometries, only one of which is displayed. Ellipsoids are set at 50% probability; hydrogen atoms and some ellipsoids have been omitted for clarity. Selected bond lengths (Å) and angles (deg) in **3**: B1–N1 1.5254(18), B1–C2 1.5542(19), N1–C1 1.4744(16), C1–C2 1.4280(18), Rh1–B1 2.2837(15), Rh1–N1 2.1290(11), Rh1–C1 2.0369(12), Rh1–C2 2.1358(13); N1–B1–C2 87.42(10), C1–N1–B1 88.78(10). In **4**: B1–C3 1.504(2), B1–C2 1.5170(18), N1–C1 1.3892(16), N1–C4 1.3808(15), C1–C2 1.3710(17), C3–C4 1.3611(17); C2–B1–C3 110.71(11), C4–N1–C1 117.69(10).

previously reported 1,4-azaborinines.[11] The phenyl ring is positioned roughly perpendicular to the azaborinine ring (the dihedral angle between the two rings is 82.20°), and the 1,4-azaborinine ring itself is planar. The four-membered ring of **3** is distorted, showing two longer bonds (B1–C2, 1.5542(19) Å; N1–C1, 1.4744(16) Å) and two shorter bonds (B1–N1, 1.526(2) Å; C2–C1, 1.425(2) Å), although the latter two distances indicate significant lengthening compared with the B≡N and C≡C triple bonds of the substrates. This distortion is typical of rhodium η^4-1,2-azaborete complexes[11] and other rhodium complexes of boron heterocycles.[17,18]

To further probe the scope of the sequential reaction, we employed ethynylferrocene, a monosubstituted polar alkyne, as a substrate. As previously reported, the stoichiometric reaction of **1** and **2** in the presence of ethynylferrocene resulted in the formation of azaborete **5**.[16] Gratifyingly, the reaction of **5** with acetylene proceeded smoothly to furnish 2-ferrocenyl-1,4-azaborinine **6** in 55% yield (Scheme 1). Notably, the reaction of **1** with ethynylferrocene alone in the presence of **2** as a catalyst led exclusively to 1,2-di-*tert*-butyl-4,6-diferrocenyl-1,2-azaborinine.

6 was isolated as an air-stable orange solid displaying a singlet at δ = 46 ppm in its ^{11}B NMR spectrum, which is shifted significantly downfield with respect to that in **5** (δ = 23.5 ppm). The ^1H NMR spectrum of **6** showed characteristic resonances for the ferrocenyl and azaborinine rings as multiplets at δ = 4.38–3.94 and 7.75–6.63 ppm, respectively. The C=C stretching frequencies of the azaborinine ring were observed in the IR spectrum, and the presence of both *tert*-butyl and ferrocenyl groups was confirmed by ^{13}C NMR spectroscopy.

The proposed structure of **6** was confirmed by crystallographic studies (Figure 3). The average B–C and N–C bond distances (1.510 and 1.388 Å, respectively) are slightly shorter than those reported for 1,2-di-*tert*-butyl-4,6-diferrocenyl-1,2-azaborinine (1.523(4) and 1.410(3) Å, respectively).[16] The azaborinine ring is slightly twisted from planarity, with an average displacement of the ring atoms of 0.02 Å, as a result of

DOI: 10.1021/jacs.6b04128
J. Am. Chem. Soc. 2016, 138, 8212–8220

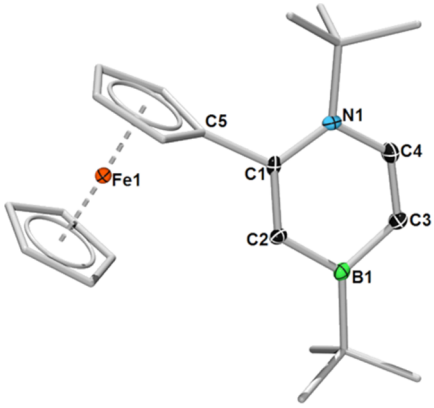

Figure 3. Molecular structure of 1,4-di-*tert*-butyl-2-ferrocenyl-1,4-azaborinine (**6**). The thermal ellipsoids of the *t*Bu, ferrocenyl ring, and hydrogen atoms have been omitted for clarity. Thermal ellipsoids are displayed at the 50% probability level. Selected bond lengths (Å) and angles (deg): B1−C2 1.516(2), B1−C3 1.505(2), N1−C1 1.397(1), N1−C4 1.379(2), C1−C2 1.372(2), C3−C4 1.356(2); C2−B1−C3 111.1(1), C4−N1−C1 118.0(1).

the steric congestion imposed by the bulky *N*-*t*Bu and ferrocenyl substituents.

To further improve our understanding of the synthesis of 1,4-azaborinines, a rhodium η^4-1,2-azaborete compound formed through the reaction of **1** and acetylene ([η^4-1,2-{B(*t*Bu)N(*t*Bu)C(H)C(H)}RhCl(P*i*Pr$_3$)])[11] was reacted with 4,4,5,5-tetramethyl-2-ethynyl-1,3,2-dioxaborolane (Bpin) and also 4-ethynyl-*N*,*N*-bis(4-methoxyphenyl)aniline, resulting in the formation of **7** and **8**, respectively (Scheme 2). Surprisingly,

Scheme 2. Synthesis of Substituted 1,4-Azaborinines 7 and 8

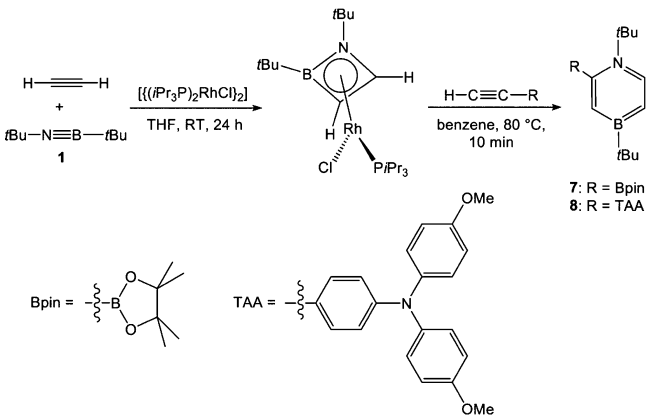

the reactions with the same rhodium azaborete complex and phenylacetylene or ethynylferrocene yielded 1,4-azaborinines also with substituents at the 2-position (as in Scheme 1). This indicates that the regiochemistry of the products is invariant to changes in the order of addition of reagents. Both **7** and **8** adopt a relatively planar structure in the solid state (see Figure S1 and Figure 4, respectively) with bond angles and distances falling within the typical ranges for 1,4-azaborinine compounds.

Synthesis of Bis- and Tris-1,4-azaborinines. In order to further extend the scope of the products available through sequential addition, reactions involving diynes were carried out, culminating in the synthesis of a bis-1,4-azaborinine (Scheme 3). The reaction of **1** and 1,4-diethynylbenzene in the presence of **2** furnished the dirhodium bis(η^4-1,2-azaborete) complex **9**

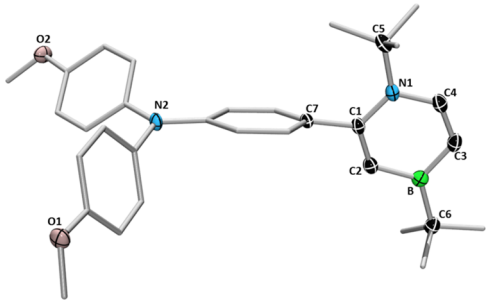

Figure 4. Molecular structure of 4-(1,4-di-*tert*-butyl-1,4-azaborinin-2-yl)-*N*,*N*-bis(4-methoxyphenyl)aniline (**8**). The thermal ellipsoids of the methyl, phenyl, and hydrogen atoms have been omitted for clarity. Thermal ellipsoids are displayed at the 50% probability level. Selected bond lengths (Å) and angles (deg): B−C3 1.503(3), B−C2 1.514 (3), N1−C1 1.385(2), N1−C4 1.387(3), C1−C2 1.372 (3), C3−C4 1.355(3) C1−C7 1.495 (3); C2−B1−C3 110.2 (2), C4−N1−C1 117.6(2).

Scheme 3. Synthesis of Bis-1,4-azaborinines 10 and 11

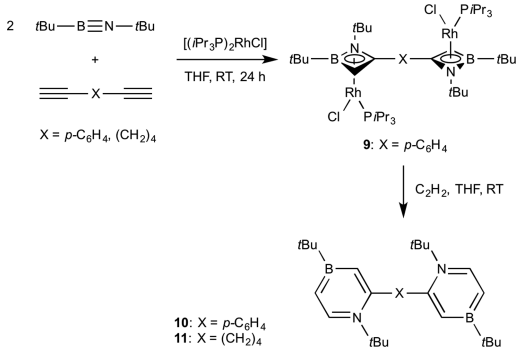

in moderate yield (24%). Subsequent reaction with acetylene gave the 1,4-phenylene-bridged bis-1,4-azaborinine **10** in 43% yield. To our knowledge, very few examples of bis(BN)-azaborinine compounds have been reported beyond a fused bis(BN-phenanthrene)azaborinine[19] and, more recently, a tolan analogue of bis(azaborinine) systems.[20] Compound **10** is stable in air at temperatures up to 110 °C in toluene.

The ^{11}B NMR spectra of **9** and **10** display signals at δ = 26 and 46 ppm, respectively, indicative of the formation of the Rh−azaborete and azaborinine compounds. The ^{1}H NMR spectrum of **10** reveals the presence of aromatic protons at δ = 6.61−7.84 ppm along with the presence of four inequivalent *tert*-butyl groups, clearly confirming the presence of *cis* and *trans* atropisomers in solution. Unfortunately, variable-temperature ^{1}H NMR spectroscopy did not provide any further information about the interconversion between the *cis* and *trans* atropisomers.[21] The structure of **10** shows a *trans*-anti orientation with dihedral angles of approximately 68° between the spacer (phenyl) and azaborinine units, which is significantly more acute than found in the all-organic analogue (93°).[21] The geometries of the azaborinine rings in **10** resemble those of **6**, displaying B−C separations of 1.511(3) and 1.517(2) Å, and NC distances of 1.378(2) and 1.394(2) Å. Interestingly, the length of 1.499(2) Å for the carbon−carbon bond connecting the NCC and phenyl rings is comparable to that observed for the corresponding C−C single bond linking the two sp^2-hybridized C atoms in butadiene (1.483(1) Å).[22] Reactions of 1,7-octadiyne with **1** and **2** led to bis-1,4-azaborinine **11** in moderate yield after final acetylene insertion. The presence of a

DOI: 10.1021/jacs.6b04128
J. Am. Chem. Soc. 2016, 138, 8212−8220

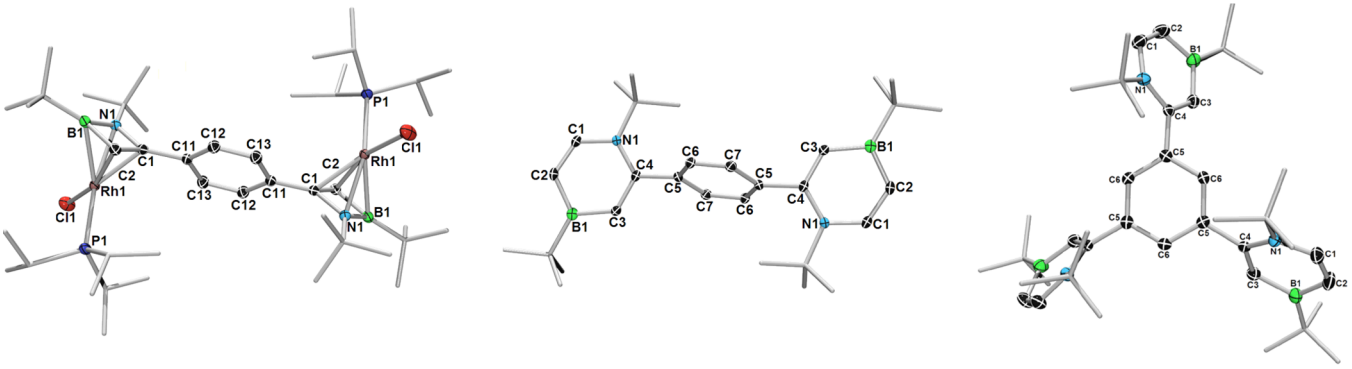

Figure 5. Molecular structures of 1,4-phenylene-bridged bis(η^4-1,4-azaborete) complex **9**, bis-1,4-azaborinine **10**, and tris-1,4-azaborinine **12**. The thermal ellipsoids of the *t*Bu, *i*Pr, and hydrogen atoms have been omitted for clarity. Thermal ellipsoids are displayed at the 50% probability level. Selected bond lengths (Å) and angles (deg) in **9**: B1−N1 1.541(2), B1−C2 1.533(2), N1−C1 1.4685(19), C1−C2 1.422(2), Rh1−B1 2.2784(18), Rh1−N1 2.1212(13), Rh1−C1 2.0369(12), Rh1−C2 2.1495(15); N1−B1−C2 87.67(12), C1−N1−B1 87.67(11). In **10**: B1−C3 1.517(2), B1−C2 1.511(3), N1−C1 1.378(2), N1−C4 1.394(2), C1−C2 1.356(2), C3−C4 1.365(2), C4−C5 1.499(2); C2−B1−C3 110.52(15), C4−N1−C1 118.05(14). In **12**: B1−C3 1.517(4), B1−C2 1.506(4), N1−C1 1.370(3), N1−C4 1.390(3), C1−C2 1.376(3), C3−C4 1.351(4), C4−C5 1.493(3); C2−B1−C3 111.0(2), C4−N1−C1 118.18(19).

^{11}B NMR resonance at δ = 46.0 ppm is consistent with the formation of a 1,4-azaborinine, while the ^{1}H NMR resonances for the *t*Bu groups at δ = 1.49 and 0.99 ppm indicate a highly symmetrical compound.

Single crystals of **9** and **10** suitable for X-ray diffraction were obtained from a pentane solution at −30 °C. The solved structures are presented in Figure 5. Single crystals of **11** suitable for X-ray diffraction analysis were grown, but the centrosymmetric nature of **11** resulted in substantial disorder. For the sake of confirming the structural assignment of **11**, the disordered structure is given in Figure S2 (see the Supporting Information for details).

With the optimized conditions determined, we next turned our attention to the synthesis of a tris-1,4-azaborinine through reactions involving 1,3,5-triethynylbenzene. These reactions yielded compound **12**, which was characterized by comparison of its spectroscopic data with those of related compounds reported here. The ^{11}B NMR spectrum of **12** shows the presence of a single resonance at δ = 47.5 ppm, which is in good agreement with the data for other 1,4-azaborinines. The ^{1}H NMR spectrum of **12** shows four resonances for the *B*- and *N*-*t*Bu protons at δ = 1.54 (18H), 1.45 (9H), 1.00 (9H), and 0.99 (18H) ppm, the latter two signals being those from the *N*-*t*Bu protons. This suggests that in solution one BN-containing ring is flipped relative to the other two.

Crystals of **12** were obtained by cooling a concentrated pentane solution to −30 °C. The solid-state structure of **12** (Figure 5) confirms the structural inferences made on the basis of the spectroscopic data. The molecule crystallizes in the triclinic space group *P*1 and thus lies on a crystallographic inversion center. The bond distances in the six-membered azaborinine ring are consistent with previously reported bond lengths for mono- and bis-1,4-azaborinines. The dihedral angles of 58.93° between the phenyl and azaborinine units are slightly smaller than in **10**.

Computational Mechanistic Studies. Density functional theory calculations were performed to model the formation of Rh−azaborete complex **3** from the reaction of phenylacetylene and *t*BuB≡N*t*Bu (**1**) with $[RhCl(PiPr_3)_2]_2$ as well as the onward reaction of **3** with acetylene to form 2-phenyl-1,4-azaborinine **4**.[23] Alternative regioselectivities were also considered in order to account for the selective formation of this product isomer. All of the geometries were optimized with the BP86 functional, and the reported free energies incorporate corrections for benzene solvent (PCM approach) and dispersion (Grimme's D3 parameter set) (see the Supporting Information for full details).

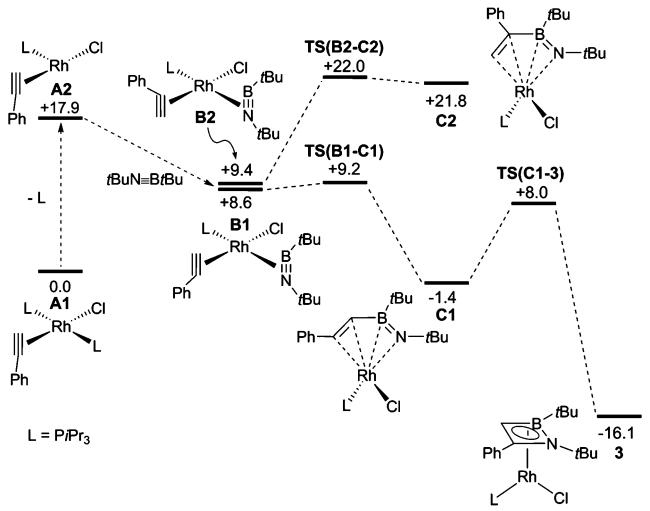

Figure 6. Computed free energy profile (BP86-D3(C_6H_6)//BP86, in kcal/mol) for the formation of Rh−azaborete complex **3** from *trans*-$[RhCl(PiPr_3)_2(\eta^2$-PhC≡CH)] (**A1**) and iminoborane **1**. The alternative B−C(Ph) coupling to give **C2** is also shown.

The reaction profile for the formation of **3** is shown in Figure 6 and starts from the intermediate *trans*-$[RhCl(PiPr_3)_2(\eta^2$-PhC≡CH)] (**A1**), which may be formed upon opening of the $[RhCl(PiPr_3)_2]_2$ dimer in the presence of PhC≡CH. All subsequent free energies are quoted relative to the combined energies of **A1** and the other reagents set to 0.0 kcal/mol. As expected, the *cis* isomer of **A1** (G = +15.4 kcal/mol) is less stable as a result of the presence of two adjacent bulky $PiPr_3$ ligands. In addition, iminoborane binding is not competitive at this stage, with $[RhCl(PiPr_3)_2(\eta^2$-*t*BuB≡N*t*Bu)] being high in energy as either its *trans* isomer (G = +19.5 kcal/mol) or *cis* isomer (G = +16.8 kcal/mol), reflecting the additional steric encumbrance arising from the *t*Bu substituents. $PiPr_3$/

DOI: 10.1021/jacs.6b04128
J. Am. Chem. Soc. 2016, 138, 8212−8220

iminoborane substitution in **A1** can proceed via [RhCl(P*i*Pr$_3$)-(η^2-PhC≡CH)] (**A2**) at +17.9 kcal/mol and leads to the relatively accessible species [RhCl(P*i*Pr$_3$)(η^2-*t*BuB≡N*t*Bu)(η^2-PhC≡CH)] (**B**), in which both the alkyne and the iminoborane lie approximately perpendicular to the Rh coordination plane. Two rotamers of **B** were located, with that in which the C(H) group lies adjacent to the *t*BuB group (**B1**) being slightly more stable (G = +8.6 kcal/mol). The iminoborane ligand in these structures binds in an unsymmetrical fashion (**B1**: Rh−N = 2.20 Å, Rh−B = 2.25 Å; see Figure 7) with the N center lying in the square-planar

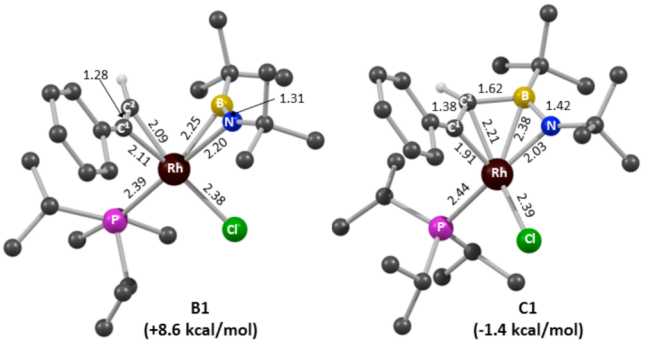

Figure 7. Computed structures of intermediates **B1** and **C1**. Selected distances are in Å, and H atoms (with the exception of that derived from the terminal alkyne position) have been omitted for clarity.

coordination plane. This appears to be an electronic preference arising from the greater Lewis basicity of the N center, as a similar distortion is retained in the computed structure of the small model complex [RhCl(PMe$_3$)(η^2-MeB≡NMe)(η^2-HC≡CH)]. From **B1** a very facile B−C(H) bond coupling can be accessed via **TS(B1−C1)** (G = +9.2 kcal/mol) that forms **C1** at −1.4 kcal/mol. The alternative rotamer, **B2** (G = +9.4 kcal/mol), has the C(Ph) group adjacent to *t*BuB and thus is set up for B−C(Ph) bond coupling; however, this process has a much higher barrier (via **TS(B2−C2)** at +22.0 kcal/mol) and is strongly endergonic, giving **C2** at +21.8 kcal/mol. Transition states for the potential N−C bond coupling processes were also located from **B1** and **B2** but were found to be even higher in energy (G > 33 kcal/mol; see the Supporting Information).

The formation of **C1** can be considered as an oxidative coupling proceeding with B−C(H) bond formation to give a Rh^{3+} species. The {(Ph)C═C(H)−(*t*Bu)B═N(*t*Bu)} moiety is therefore considered as a dianionic ligand with formal negative charges on the C(Ph) and B centers. The major interaction with the Rh center occurs through short Rh−N and Rh−C(Ph) σ bonds (2.03 and 1.91 Å, respectively; see Figure 7), and these are supported by additional Rh−C(H) and Rh−B contacts of 2.21 and 2.38 Å, respectively. The C(Ph)−C(H) and B−N distances of 1.38 and 1.42 Å, respectively, indicate significant double-bond character with little delocalization across the central B−C(H) bond (1.62 Å). N−C(Ph) bond formation can then proceed from **C1** and occurs via **TS(C1−3)** with a modest barrier of 9.4 kcal/mol. This reductive coupling process forms complex **3** at −16.1 kcal/mol in which a neutral 1,2-azaborete ligand is bound to a Rh$^+$ center. The computed structure of **3** agrees well with that determined experimentally, the main discrepancy being a slight overestimation of the distances between Rh and the azaborete ligand by ca. 0.04 Å (see the Supporting Information).

Overall, the formation of complex **3** from intermediate **A1** is computed to proceed via P*i*Pr$_3$/iminoborane substitution and sequential B−C(H) and N−C(Ph) bond-coupling events. The highest point on the profile is at +17.9 kcal/mol and corresponds to the species [RhCl(P*i*Pr$_3$)(η^2-PhC≡CH)] (**A2**) formed upon loss of P*i*Pr$_3$ from **A1**. The subsequent B−C(H) coupling is highly selective, with the alternative B−C(Ph) coupling (and the potential C(R)−N couplings) being clearly higher in energy. B−C(H) coupling in **B1** is computed to have a much lower barrier than N−C(Ph) coupling in **C1**, although the latter is more thermodynamically favorable, presumably because it is driven by the formation of the delocalized 1,2-azaborete ligand.

Several possibilities were considered for the onward reaction of the 1,2-azaborete complex **3** with acetylene to form the 1,4-azaborinine product. Pathways were characterized for B−N bond cleavage of the azaborate moiety either directly in **3** or after the facile addition of acetylene to give intermediate **D**; details of these processes (and those for the related B−C bond cleavage processes in **3** and **D**) are provided in Scheme S2. However, the most accessible pathway (see Figures 8 and 9, which also provide the labeling scheme employed) involves the

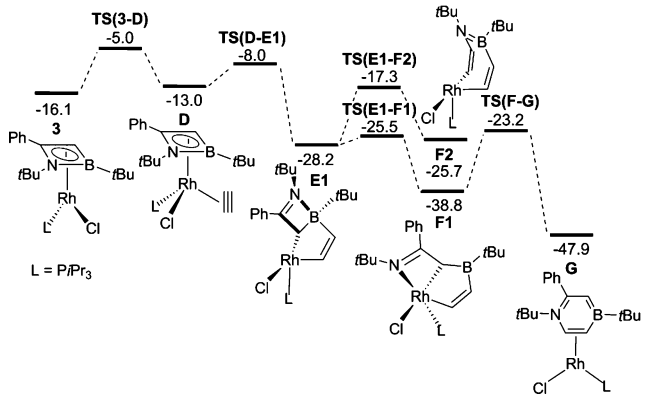

Figure 8. Computed free energy profile (BP86-D3(C_6H_6)//BP86, in kcal/mol) for the formation of rhodium η^2-(*C*,*C*)-1,4-azaborinine complex **G** from 1,2-azaborete complex **3** and acetylene. The alternative B−C(H) bond cleavage in **E1** to form **F2** is also indicated.

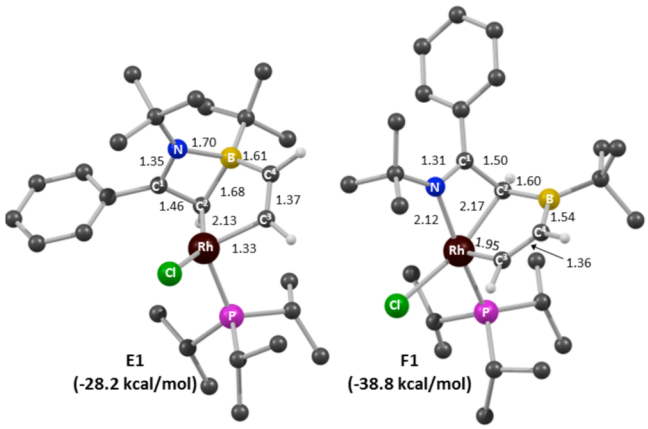

Figure 9. Computed structures of intermediates **E1** and **F1**. Selected distances are in Å, and H atoms (with the exception of those derived from the alkyne positions) have been omitted for clarity.

DOI: 10.1021/jacs.6b04128
J. Am. Chem. Soc. 2016, 138, 8212−8220

formation of **D** followed by insertion of the alkyne into the Rh−B bond with a barrier of only 5 kcal/mol to produce intermediate **E1** at −28.2 kcal/mol. Transition states for the alternative insertions into the Rh−C^1(Ph) and Rh−C^2(H) bonds proved to be significantly higher in energy (see Scheme S2). **E1** features a five-membered metallaboracycle fused with the still-intact imine-stabilized borane moiety, which is bound in an η^1 fashion to Rh via C^2 (Rh−C^2 = 2.13 Å; Figure 9). The B−N bond in **E1** is now significantly elongated to 1.70 Å, and its cleavage readily occurs via **TS(E1-F1)** with a barrier of only 2.7 kcal/mol to form **F1** at −38.8 kcal/mol. This bond cleavage is accompanied by a rotation about the C^1(Ph)−C^2(H) bond of the azaborete moiety such that the N(*t*Bu) group migrates back onto the Rh center. The Rh−C^2 bond noted in **E1** is therefore retained such that **F1** features a new bicyclic structure with {RhN(*t*Bu)C^1(Ph)C^2(H)} and {RhC^2(H)B(*t*Bu)C^4(H)-C^3(H)} rings. These fold along the shared Rh−C^2 bond to give a tridentate ligand that is bound in a facial manner, with overall square-pyramidal coordination at Rh. C^3−N bond-forming reductive coupling in **F1** proceeds with a barrier of 15.6 kcal/mol to give **G**, in which the 2-phenyl-1,4-azaborinine product is bound in an η^2 fashion to the {RhCl(P*i*Pr_3)} fragment. Displacement of the azaborinine by P*i*Pr_3 forms the free product and *trans*-RhCl(P*i*Pr_3)$_2$ at −46.7 kcal/mol, to which PhCCH can bind to reform **A1** at −71.8 kcal/mol.

Intermediate **E1** may also potentially undergo a B−C^2 bond cleavage that could ultimately lead to the alternative 1,2-azaborinine product. Characterization of this process, however, revealed it to be disfavored both kinetically ($\Delta G^{\ddagger}$ = 10.9 kcal/mol) and thermodynamically, with the putative seven-membered metallacycle **F2** lying 13.1 kcal/mol above **F1** (and 2.5 kcal/mol above **E1**). This preference for B−N bond cleavage in **E1** is consistent with the regioselective formation of the 1,4-azaborinine product.

The computed reaction profile for the formation of 1,4-azaborinine adduct **G** from **3** and acetylene is strongly exergonic (ΔG = −31.8 kcal/mol) and involves a series of low-energy processes of which the largest barrier is 15.6 kcal/mol, corresponding to the final N−C bond-coupling event. In comparison, the formation of the 1,2-azaborete is less exergonic (ΔG = −16.1 kcal/mol) and, aside from the initial P*i*Pr_3 dissociation, has lower barriers to its formation. The regioselectivity for 2-phenyl-1,4-azaborinine formation derives from the selective B−C(H) reductive coupling seen in intermediate **B1** in conjunction with the selective oxidative cleavage of the B−N bond in **E1**.

It is of interest to contrast the mechanism proposed here for 1,4-azaborinine formation with those put forward in the literature for Rh- and Ir-catalyzed alkyne trimerization.[24] The latter are initiated via oxidative coupling of two alkynes to give planar metallacyclopentadiene intermediates, equivalent to the (nonplanar) intermediate **C1** proposed here. Onward reaction with a third alkyne can involve a direct [4 + 2] cycloaddition or insertion to give a metallacycloheptatriene, from which C−C reductive coupling forms the arene product. This latter mechanism can feature a metallabicyclo[3.2.0]heptatriene intermediate that is isoelectronic with **F1**;[25] indeed, such a species has been characterized experimentally.[26] An all-carbon analogue of bicyclic **E1** has not been proposed, however, and this may reflect the fact that **E1** is formed via reaction of acetylene with the 1,2-azaborete ligand in **3**. In contrast, the isoelectronic cyclobutadiene complex, if it forms, is thought to lie off the catalytic cycle for alkyne trimerization. The regioselective formation of the 1,4-azaborinines formed here contrasts with the observation of 1,2-azaborinines seen in the direct reaction of ethynylferrocene with *t*BuB≡N*t*Bu, indicating a significant role of substituent effects in dictating the selectivity.[11] Work to understand these different outcomes is currently underway.

Electrochemical and Photophysical Characterization of 8. In view of the results of the recently published 1,2-azaborinine **13** and **Ref**[27] (Figure 10), we investigated the 1,4-azaborinine **8** by cyclic voltammetry and UV/vis/NIR absorption and emission spectroscopy in order to elucidate the influence of the azaborinine isomers on the electronic properties in such donor−acceptor chromophores.

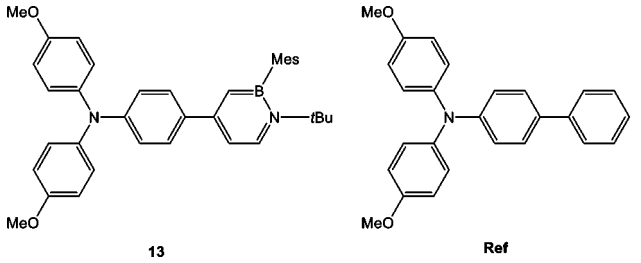

Figure 10. Structures of **13** and **Ref**.

Electrochemical Properties. The cyclic voltammograms of **8** (Figure 11A) show a first oxidation wave at 256 mV vs ferrocene/ferrocenium (Fc/Fc^+) as an internal standard in CH_2Cl_2/0.15 M tetrabutylammonium hexafluorophosphate (TBAH). The first oxidation can be assigned to a one-electron oxidation of the nitrogen atom in the triarylamine (TAA)[26] unit and is reversible even under thin-film conditions. In the square-

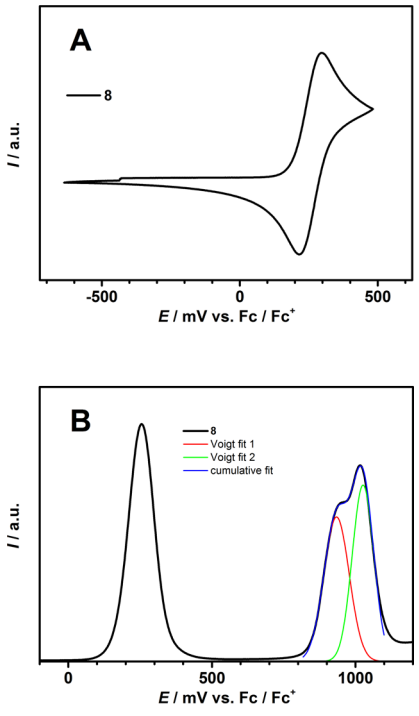

Figure 11. (A) Cyclic voltammogram of **8** in CH_2Cl_2 (TBAH) at a scan rate of 100 mV s^{-1}. (B) Square-wave voltammogram (black line) of **8** in CH_2Cl_2 at a scan rate of 50 mV s^{-1}. Voigt fits (red and green lines) and the cumulative fit (blue line) are also shown.

DOI: 10.1021/jacs.6b04128
J. Am. Chem. Soc. 2016, 138, 8212−8220

Table 1. Optical Steady-State and Emission Decay Data for 8 in MeCN, CH_2Cl_2, and Toluene

solvent	$\tilde{\nu}_{abs}$/cm^{-1} (nm)	ε/M^{-1} cm^{-1}	$\tilde{\nu}_{fl}$/cm^{-1} (nm)	ϕ_f	τ_{fl}/ns
MeCN	32900 (304); 38300 (261)[a]	23900	20600 (485)	0.33 ± 0.014	5.62
CH_2Cl_2	32600 (307); 38600 (259)[a]	23000	21700 (461)	–[c]	–[c]
toluene	32500 (308); –[b]	23700	23600 (424)	0.10 ± 0.001	0.68

[a]Less intense maximum. [b]Could not be measured because of insufficient solvent transparency. [c]Could not be measured because of decomposition.

wave voltammogram (Figure 11B), an additional double peak associated with irreversible oxidation processes at higher potential (800−1100 mV vs Fc/Fc^+) is visible (Figure S4). A fit with two Voigt functions revealed two processes at 934 and 1026 mV vs Fc/Fc^+. We assume that one of these potentials refers to the second oxidation of the TAA unit and the other one to oxidation of the 1,4-azaborinine unit. However, a discrete assignment is impossible.

The electrochemical behavior of 1,4-azaborinine **8** is similar to that of 1,2-azaborinine **13** and the all-carbon compound **Ref**, but the first oxidation wave is at a ca. 30 mV higher potential in **8** (**13**: 224 mV; **Ref**: 228 mV), indicating a greater electron-withdrawing strength of the 1,4-azaborinine unit compared with the 1,2-azaborinine unit. In addition, the two peaks around 800−1100 mV vs Fc/Fc^+ in **8** are slightly more separated than those in **13** and **Ref**.

UV/Vis/NIR Spectroscopy. The steady-state absorption spectra of **8** in MeCN, CH_2Cl_2, and toluene are shown in Figure 13. These absorption spectra display two $\pi-\pi^*$ absorption bands typical of TAA.[28,29] The first absorption band at ca. 32800 cm^{-1} is caused by a HOMO → LUMO ($S_1 \leftarrow S_0$) transition and the second at ca. 38600 cm^{-1} by a HOMO → LUMO+1 ($S_2 \leftarrow S_0$) transition (Table 1).[29] Both peaks depend on the solvent polarity. They are broader in nonpolar solvents and show a weak negative solvatochromism. The $S_1 \leftarrow S_0$ transition rises from 32500 cm^{-1} in toluene to 32900 cm^{-1} in MeCN and the $S_2 \leftarrow S_0$ transition from 38300 cm^{-1} in MeCN to 38600 cm^{-1} in CH_2Cl_2, which indicates some charge transfer (CT) character of both electronic transitions. This absorption behavior is also in good agreement with calculations of the frontier molecular orbitals (Figure 12), which were carried out using the Gaussian 09 software suite (see the Supporting Information for details). The ground-state molecular geometries were optimized at the B3LYP/6-311G(d) level of theory, and were found to be true minima through frequency analyses. The HOMO is TAA-localized, while the LUMO and the LUMO+1 show more contribution from the azaborinine unit. Excitation from a HOMO to the LUMO or LUMO+1 should be associated with a change in dipole moment, and consequently, both transitions depend on the solvent polarity.

The absorption spectra of **13** and **Ref** show quite similar characteristics, but in the case of **8** the difference in energy between the two $\pi-\pi^*$ absorptions (and thus the difference in the energies of the LUMO and LUMO+1) are smaller than in **13**. While in MeCN the two absorption maxima of **8** are separated by 5400 cm^{-1}, in **13** they are only 3400 cm^{-1} apart. In **Ref** the maxima are so close together that only a broad band with a shoulder in the lower-wavelength regime is visible. The $S_2 \leftarrow S_0$ transition of **8** illustrates another difference. Whereas the $S_2 \leftarrow S_0$ transition of **8** is dependent on the polarity of the solvent, in **13** and **Ref** nearly no CT is visible and the transition is independent of the solvent.

Emission spectra of **8** were measured in MeCN, CH_2Cl_2, and toluene (Figure 13).[28,30] The fluorescence spectra were recorded by excitation at the absorption maxima, but excitation at lower excitation wavenumbers resulted in the same emission. The emission maxima of **8** shift from 20600 cm^{-1} in toluene and 21700 cm^{-1} in CH_2Cl_2 to 23600 cm^{-1} in MeCN. This strong positive solvatochromism fluorescence of **8** is accompanied by a large apparent Stokes shift (8900 cm^{-1} in toluene and 12300 cm^{-1} in MeCN), indicating a major reorganization

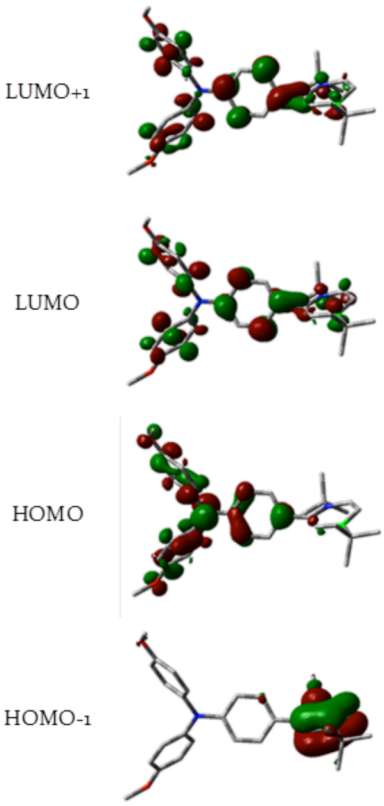

Figure 12. Isosurface plots of the HOMO−1, HOMO, LUMO, and LUMO+1 for **8**.

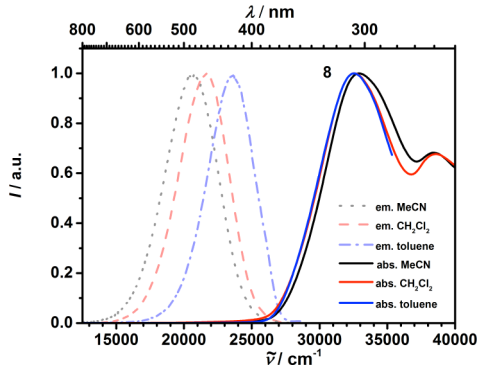

Figure 13. Normalized absorption spectra (solid lines) and emission spectra (dashed lines) of **8** in MeCN (black), CH_2Cl_2 (red), and toluene (blue).

DOI: 10.1021/jacs.6b04128
J. Am. Chem. Soc. 2016, 138, 8212−8220

of the excited state in the more polar solvents. The fact that there is only weak solvatochromism in the absorption spectra but strong solvatochromism in the fluorescence spectra speaks for a vanishing ground-state dipole moment but a large excited-state dipole moment.

Fluorescence lifetimes were measured by time-correlated single photon counting with excitation at 31600 cm^{-1}. Compound **8** shows a fluorescence lifetime of a few nanoseconds with a monoexponential decay (Table 1). The fluorescence lifetime was also found to be dependent on the solvent polarity: in the polar solvent MeCN the excited state is stabilized and the lifetime rises to 5.62 ns, whereas in toluene the lifetime drops to 0.68 ns (Figure S3). The fluorescence quantum yield (QY) of **8** is surprisingly low (see Table 1). In MeCN, **8** shows a QY of 33%, which in toluene drops to 10%. Because of slow decomposition of **8** in CH_2Cl_2, we were unable to perform accurate fluorescence lifetime or fluorescence quantum yield measurements in this solvent.

The emission maximum of **8** is between those of 1,2-azaborinine **13** and the all-carbon analogue **Ref** (e.g., in MeCN: **13**, 19500 cm^{-1}; **8**, 20600 cm^{-1}; **Ref**, 21400 cm^{-1}). The Stokes shift of **8** is significantly higher and the fluorescence lifetime of **8** is shorter than those of **13** and **Ref** (both in toluene and MeCN). Here the all-carbon chromophore has the longest lifetime in the respective solvent (e.g., in MeCN: **Ref**, 8.20 ns; **13**, 7.34 ns; **8**, 5.62 ns). However, the largest difference in the emission behavior of these compounds is the fluorescence quantum yield. The 1,4-azaborinine compound **8** was found to be significantly less fluorescent than the 1,2-azaborinine compound and the all-carbon analogue (e.g., in toluene: **13**, 0.47%; **Ref**, 0.30%; **8**, 0.10%).

CONCLUSION

We have demonstrated the utility of iminoboranes for the construction of 1,4-azaborinines with a range of architectures. The scope of the reaction with respect to the inclusion of terminal alkynes is broad and allows the use of substrates with functional groups not tolerated by previous synthetic routes to 1,4-azaborinines. This methodology has also enabled the synthesis and characterization of bis- and (the first) tris-1,4-azaborinines, which are BN analogues of *p*-terphenyl and 1,3,5-triphenylbenzene, respectively. The structural, spectroscopic, and chemical data presented in this work were fully supported by high-level calculations. Our current efforts are directed toward expanding the scope of this reaction in the context of 1,4-azaborinines. The results described herein further open the door to the wide and uncharted field of BN heterocycle chemistry, and it is anticipated that this study will provide new avenues in BN-doped molecular architectures of importance to medicinal and materials chemistry.

ASSOCIATED CONTENT

Supporting Information

The Supporting Information is available free of charge on the ACS Publications website at DOI: 10.1021/jacs.6b04128.

Procedures and additional data (PDF)
Computed Cartesian coordinates (XYZ)
Crystallographic data for **3**, **4**, **6**, **8**−**10**, and **12** (CIF)

AUTHOR INFORMATION

Corresponding Authors

*s.a.macgregor@hw.ac.uk
*christoph.lambert@uni-wuerzburg.de
*h.braunschweig@uni-wuerzburg.de

Present Address

⊥Department of Inorganic & Physical Chemistry, Indian Institute of Science, Bangalore 560012, India.

Notes

The authors declare no competing financial interest.

ACKNOWLEDGMENTS

This work was financially supported by the Deutsche Forschungsgemeinschaft (DFG grant to H.B.). K.G. thanks the Alexander von Humboldt Foundation for a postdoctoral fellowship. N.A.B. thanks the EPSRC and Heriot-Watt University for a DTP studentship.

REFERENCES

(1) (a) Lepeltier, M.; Lukoyanova, O.; Jacobson, A.; Jeeva, S.; Perepichka, D. F. *Chem. Commun.* **2010**, *46*, 7007−7009. (b) Bosdet, M. J. D.; Piers, W. E. *Can. J. Chem.* **2009**, *87*, 8−29. (c) Campbell, P. G.; Marwitz, A. J. V.; Liu, S.-Y. *Angew. Chem., Int. Ed.* **2012**, *51*, 6074−6092. (d) Fritsch, A. J. *Chem. Heterocycl. Compd.* **1977**, *30*, 381−440.

(2) (a) Dewar, M. J. S.; Kubba, V. P.; Pettit, R. *J. Chem. Soc.* **1958**, 3073−3076. (b) Dewar, M. J. S.; Dietz, R. *J. Chem. Soc.* **1959**, 2728−2730. (c) Dewar, M. J. S.; Marr, P. A. *J. Am. Chem. Soc.* **1962**, *84*, 3782. (d) Davies, K. M.; Dewar, M. J. S.; Rona, P. *J. Am. Chem. Soc.* **1967**, *89*, 6294−6297.

(3) White, D. G. *J. Am. Chem. Soc.* **1963**, *85*, 3634−3636.

(4) (a) Ashe, A. J., III; Fang, X. *Org. Lett.* **2000**, *2*, 2089−2091. (b) Ashe, A. J., III; Fang, X.; Fang, X.; Kampf, J. W. *Organometallics* **2001**, *20*, 5413−5418.

(5) (a) Jaska, C. A.; Emslie, D. J. H.; Bosdet, M. J. D.; Piers, W. E.; Sorensen, T. S.; Parvez, M. *J. Am. Chem. Soc.* **2006**, *128*, 10885−10896. (b) Bosdet, M. J. D.; Piers, W. E.; Sorensen, T. S.; Parvez, M. *Angew. Chem., Int. Ed.* **2007**, *46*, 4940−4943.

(6) Taniguchi, T.; Yamaguchi, S. *Organometallics* **2010**, *29*, 5732−5735.

(7) Lepeltier, M.; Lukoyanova, O.; Jacobson, A.; Jeeva, S.; Perepichka, D. F. *Chem. Commun.* **2010**, *46*, 7007−7009.

(8) (a) Liu, L.; Marwitz, A. J. V.; Matthews, B. W.; Liu, S.-Y. *Angew. Chem., Int. Ed.* **2009**, *48*, 6817−6819. (b) Abbey, E. R.; Zakharov, L. N.; Liu, S.-Y. *J. Am. Chem. Soc.* **2010**, *132*, 16340−16342. (c) Abbey, E. R.; Zakharov, L. N.; Liu, S.-Y. *J. Am. Chem. Soc.* **2011**, *133*, 11508−11511.

(9) Marwitz, A. J. V.; Matus, M. H.; Zakharov, L. N.; Dixon, D. A.; Liu, S.-Y. *Angew. Chem., Int. Ed.* **2009**, *48*, 973−977.

(10) Xu, S.; Zakharov, L. N.; Liu, S.-Y. *J. Am. Chem. Soc.* **2011**, *133*, 20152−20155.

(11) Braunschweig, H.; Damme, A.; Jimenez-Halla, J. O. C.; Pfaffinger, B.; Radacki, K.; Wolf, J. *Angew. Chem., Int. Ed.* **2012**, *51*, 10034−10037.

(12) Maitlis, P. M. *J. Chem. Soc.* **1961**, 425−429.

(13) Kranz, M.; Hampel, F.; Clark, T. *J. Chem. Soc., Chem. Commun.* **1992**, 1247−1248.

(14) (a) Agou, T.; Arai, H.; Kawashima, T. *Chem. Lett.* **2010**, *39*, 612−613. (b) Agou, T.; Kojima, T.; Kobayashi, J.; Kawashima, T. *Org. Lett.* **2009**, *11*, 3534−3537. (c) Agou, T.; Sekine, M.; Kobayashi, J.; Kawashima, T. *Chem. - Eur. J.* **2009**, *15*, 5056−5062. (d) Agou, T.; Sekine, M.; Kobayashi, J.; Kawashima, T. *Chem. Commun.* **2009**, 1894−1896.

(15) Xu, S.; Haeffner, F.; Li, B.; Zakharov, L. N.; Liu, S.-Y. *Angew. Chem., Int. Ed.* **2014**, *53*, 6795−6799.

(16) Braunschweig, H.; Geetharani, K.; Jimenez-Halla, J. O. C.; Schaefer, M. *Angew. Chem., Int. Ed.* **2014**, *53*, 3500−3504.

(17) (a) Hitchcock, P. B.; Maah, M. J.; Nixon, J. F. *J. Chem. Soc., Chem. Commun.* **1986**, 737−738. (b) Meidine, M. F.; Pombeiro, A. J. L.; Nixon, J. F. *J. Chem. Soc., Dalton Trans.* **1999**, 3041−3045.

DOI: 10.1021/jacs.6b04128
J. Am. Chem. Soc. 2016, 138, 8212−8220

(18) (a) Xu, S.; Zakharov, L. N.; Liu, S.-Y. *J. Am. Chem. Soc.* **2011**, *133*, 20152−20155. (b) Huttner, G.; Krieg, B. *Chem. Ber.* **1972**, *105*, 3437−3444. (c) Delpy, K.; Schmitz, D.; Paetzold, P. *Chem. Ber.* **1983**, *116*, 2994−2999.
(19) (a) Jaska, C. A.; Piers, W. E.; McDonald, R.; Parvez, M. J. *J. Org. Chem.* **2007**, *72*, 5234−5243. (b) Lukoyanova, O.; Lepeltier, M.; Laferrière, M.; Perepichka, D. F. *Macromolecules* **2011**, *44*, 4729−4734.
(20) Marwitz, A. J. V.; Lamm, A. N.; Zakharov, L. N.; Vasiliu, M.; Dixon, D. A.; Liu, S.-Y. *Chem. Sci.* **2012**, *3*, 825−829.
(21) Lunazzi, L.; Mazzanti, A.; Minzoni, M.; Anderson, J. E. *Org. Lett.* **2005**, *7*, 1291−1294.
(22) Marais, D. J.; Sheppard, N.; Stoicheff, B. P. *Tetrahedron* **1962**, *17*, 163−169.
(23) A computational study on the metal-free [2+2] cycloadditions of iminoboranes and alkynes indicates that such processes encounter a significant barrier. See: Bissett, K. M.; Gilbert, T. M. *Organometallics* **2004**, *23*, 5048−5053.
(24) (a) Dahy, A. A.; Koga, N. *Organometallics* **2015**, *34*, 4965−4974. (b) Guo, C.-H.; Wu, H.-S.; Hapke, M.; Jiao, H. *J. Organomet. Chem.* **2013**, *748*, 29−35. (c) Dachs, A.; Osuna, S.; Roglans, A.; Sola, M. *Organometallics* **2010**, *29*, 562−569. (d) Dachs, A.; Torrent, A.; Roglans, A.; Parella, T.; Osuna, S.; Sola, M. *Chem. - Eur. J.* **2009**, *15*, 5289−5300.
(25) For computational characterization of an equivalent process involving the reaction of a rhodapentadiene and acetonitrile, see: Orian, L.; van Stralen, J. N. P.; Bickelhaupt, F. M. *Organometallics* **2007**, *26*, 3816−3830.
(26) Paneque, M.; Poveda, M. L.; Rendon, N.; Mereiter, K. *J. Am. Chem. Soc.* **2004**, *126*, 1610−1611.
(27) Schäfer, M.; Schäfer, J.; Dewhurst, R. D.; Ewing, W. C.; Krahfuß, M.; Kuntze-Fechner, M. W.; Wehner, M.; Lambert, C.; Braunschweig, H. *Chem. - Eur. J.* **2016**, *22*, 8603−8609.
(28) Amthor, S.; Noller, B.; Lambert, C. *Chem. Phys.* **2005**, *316*, 141−152.
(29) Amthor, S.; Lambert, C. *J. Phys. Chem. A* **2006**, *110*, 1177−1189. (b) Dapperheld, S.; Steckhan, E.; Brinkhaus, K.-H. G.; Esch, T. *Chem. Ber.* **1991**, *124*, 2557−2567. (c) Seo, E. T.; Nelson, R. F.; Fritsch, J. M.; Marcoux, L. S.; Leedy, D. W.; Adams, R. N. *J. Am. Chem. Soc.* **1966**, *88*, 3498−3503. (d) Schmidt, W.; Steckhan, E. *Chem. Ber.* **1980**, *113*, 577−585.
(30) Amthor, S.; Lambert, C.; Dümmler, S.; Fischer, I.; Schelter, J. *J. Phys. Chem. A* **2006**, *110*, 5204−5214.

DOI: 10.1021/jacs.6b04128
J. Am. Chem. Soc. 2016, 138, 8212−8220